Modified Slotted Patch Antenna With Metasurface as Superstrate for Dual-Band Applications

Diptiranjan Samantaray, *Student Member, IEEE*, Sambit Kumar Ghosh, *Student Member, IEEE*, and Somak Bhattacharyya, *Senior Member, IEEE*

***Abstract*—This letter presents the design, circuit model analysis, and realization of a novel metasurface-based low-profile slotted patch antenna for dual-band applications in the C and X-bands. The antenna prototype comprises a modified slotted patch and a 7×7 array of periodic metasurface (MS) as superstrate configuration. Both the radiating patch and the MS layer have been designed over FR4 dielectric substrate while the overall dimension of the proposed antenna being $1.03\lambda_0 \times 1.03\lambda_0 \times 0.15\lambda_0$ only, where λ_0 is the free-space wavelength at 8.62 GHz. The −10 dB impedance bandwidth of the proposed antenna has been realized at two distinct frequency bands ranging from 4.18 to 4.44 GHz and 8.11 to 11.14 GHz. The fractional bandwidths of 6.1% and 35.15% have been achieved at 4.26 and 8.62 GHz, respectively. The equivalent circuit model of the proposed prototype has been sequentially developed to validate the electromagnetic simulated results. The antenna radiates in the boresight direction, with a maximum realized gain of 8.72 dBi at 10.99 GHz and radiation efficiency of 91%. The proposed prototype has also been fabricated and the experimentally measured results are in good resemblance with the simulated one.**

***Index Terms*—Metasurface (MS), microstrip, slotted annular patch, superstrate.**

I. Introduction

IN RECENT days, researchers from every corner of the world are utilizing various emerging techniques for the design and development of high-performance wireless communication systems [1], [2], [3]. Earlier, various techniques, viz., coplanar parasitic patches, stacked patches, dielectric resonators, and involvement of different types of slots, have been opted to design and develop broadband antennas [2], [3], [4], [5]. However, these antennas were bulky, complex in design, and suffered from narrow bandwidth (BW) [1], [2]. The dual-band antennas can deliver a strong and consistent wireless connection supporting numerous wireless standards, even in remote locations [4], [5]. In certain instances of antenna design, space control is a critical parameter in addition to the cost reduction [3], [4], [5].

Over the last two decades, the concept of metasurface (MS) has been introduced in various antenna designs for realizing high-performance systems such as operational BW, radiation efficiency, etc. [4], [5], [6], [7], [8], [9]. The MS structures have been used in other applications apart from the antenna designs, viz., polarization converters, absorbers, phase shifters, filters, cloaking, lensing, etc. [4], [5], [6], [7], [8], [9], [10]. Nowadays, antenna designers focus on superstrate structures for performance improvement in terms of BW, gain, and directive radiation pattern while maintaining low cross-polarization features [5], [6], [7], [9], [10], [11]. However, these antenna designs do not offer compactness due to their high-profile thickness and bulky nature [5], [6], [7], [9], [10], [11]. Furthermore, the dual-band antennas mentioned in [3] and [4] are low-profile in nature for various potential applications such as body-centric communications, energy harvesting, frequency agility, etc., but these antennas suffer from both narrow BW and low gain. Some of the reported Fabry–Perot (FP) antennas in [5], [6], and [7] achieved superior gain, although they were developed in larger dimensions on a substrate with high relative permittivity.

In this letter, an MS antenna with a planar, low-profile, compact, efficient, dual-band with improved radiation characteristics has been proposed for radar and military applications. The antenna is miniaturized by at least 0.1λ compared to other multilayered FP antennas [5], [6], [7]. The significant accomplishment of this antenna is that it provides a realized gain of 8.72 dBi while maintaining a low profile. The antenna operates at two different frequency regions, providing fractional bandwidths of 6.1% and 35.15% at 4.26 and 8.62 GHz, respectively. The analysis of this work has been further extended by studying the circuit model simulation. The circuit model has been sequentially developed to validate the impedance behavior of the proposed antenna configuration. The proposed prototype has been fabricated, and the experimentally measured results offer good agreement with the simulated ones.

II. Design of the Antenna

The presented antenna comprises a slotted patch and a 7×7 order MS structure in which the patch is formed by square annular-shaped slots at the four corners. The MS layer is integrated with unit cells where each meta-atom composes a centered patch surrounded by four rectangular strips. Both the radiating patch and the MS layer have been printed on a 1.6 mm thick FR4 dielectric layer (loss tangent = 0.025 and relative permittivity = 4.4) and separated from each other by 2.2 mm thick air spacer. The three-dimensional (3D) geometry of the proposed structure with the conventional patch and 7×7 order MS superstrate layer have been represented in Fig. 1(a)–(c). The optimization and analysis of the proposed geometry have been performed using Ansys HFSS [12]. Furthermore, the $|S_{11}|$ response of the optimized design has been compared to the

Manuscript received 30 July 2022; accepted 30 August 2022. Date of publication 8 September 2022; date of current version 5 January 2023. This work was supported in part by SERB, Govt. of India under Grant CRG/2021/000947. *(Corresponding author: Somak Bhattacharyya.)*

The authors are with the Department of Electronics Engineering, Indian Institute of Technology Banaras Hindu University, Varanasi 221005, India (e-mail: drsamantaray.rs.ece17@iitbhu.ac.in; sambitkrghosh.rs.ece17@iitbhu.ac.in; somakbhattacharyya.ece@iitbhu.ac.in).

Digital Object Identifier 10.1109/LAWP.2022.3204180

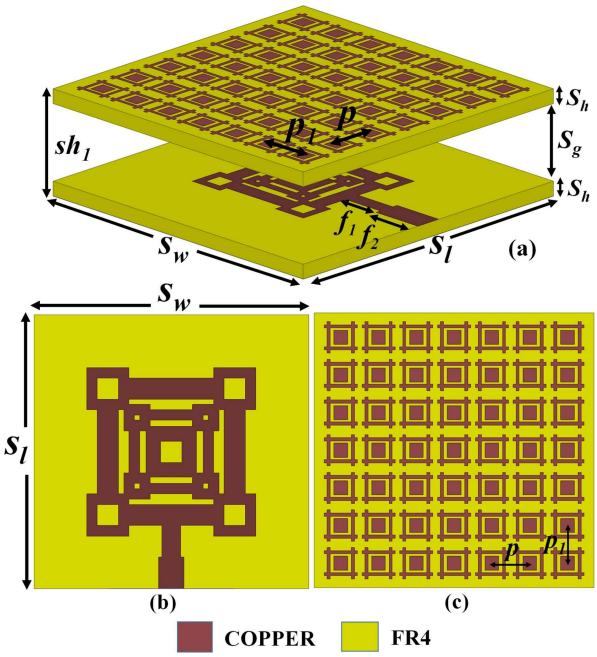

Fig. 1. (a) 3-D geometry of proposed structure. (b) Conventional patch. (c) 7×7 order MS structure [optimized parameters: $S_w = S_l = 36$ mm, $S_h = 1.6$ mm, $S_g = 2.2$ mm, $p = 5.2$ mm, $p_1 = 5$ mm].

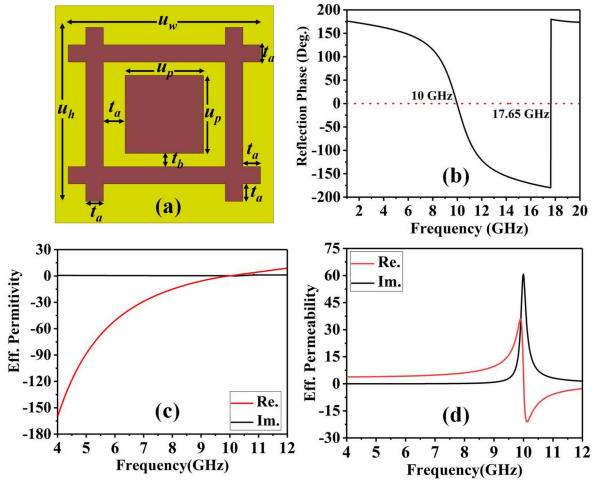

Fig. 2. (a) Unit cell (optimized parameters: $u_w = 4.4$ mm, $u_h = 4$ mm, $u_p = 2$ mm, $t_a = 0.4$ mm, $t_b = 0.2$ mm). (b) Reflection phase characteristics with respect to frequency. (c) Effective permittivity. (d) Effective permeability of the unit cell.

response achieved by the equivalent circuit model in Keysight Advanced Design System (ADS) [13].

The unit cell of the MS has been designed according to the operating wavelength and comprises a center patch surrounded by four rectangular strips of identical dimensions. The unit cell has been studied under the periodic arrangement as shown in Fig. 2(a) using Ansys HFSS [12]. The periodically arranged unit cell exhibits a 0° reflection phase at 10 and 17.65 GHz, as observed in Fig. 2(b). The variation in the reflection phase is bounded between ±180° over the frequency region 1-20 GHz, as seen in Fig. 3(b). Furthermore, the real and imaginary parts of the effective permittivity and the effective permeability have been extracted by the *S*-parameter retrieval method [14], and the

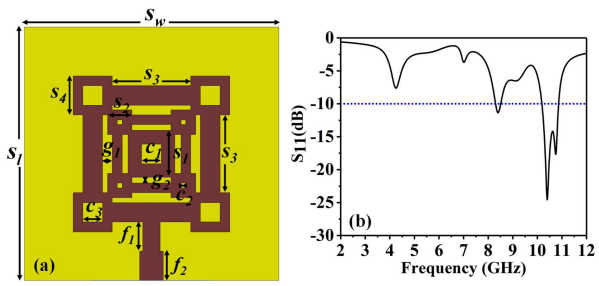

Fig. 3. (a) Radiating patch [optimized parameters: $s_1 = 4.8$ mm, $s_2 = 2.5$ mm, $s_3 = 8$ mm, $s_4 = 4$ mm, $c_1 = 2$ mm, $c_2 = 0.5$ mm, $c_3 = 2$ mm, $g_1 = 1$ mm, $g_2 = 0.6$ mm, $f_1 = 5$ mm, $f_2 = 6$ mm]. (b) Plot of S_{11} (dB) with respect to frequency.

retrieved parameters of the same have been shown in Fig. 2(c) and (d), respectively. The zero-phase reflection BWof the MS significantly influences the BW of the array of unit elements. It has also been found that the increase in equivalent inductance is responsible for enhancing BW in MS structures [15]. The equivalent input impedance of an MS unit element can be expressed as the parallel combination of the periodic pattern impedance and the grounded dielectric layer impedance. This results in the equality between the MS reflection BW and the BW of a parallel LC circuit with net inductance and capacitance of L_m and C_m , respectively, as seen from (1)

$$\mathrm{BW} = \frac{\omega_0^2 \mathrm{L_m}}{\mathrm{Z_0}} = \frac{1}{\mathrm{C_m Z_0}} \tag{1}$$

where Z_0 is the free space impedance. This implies that by lowering C_m, the MS zero-phase BW can also be enhanced, which can be accomplished by forming a wide slot gap between the central patch and the rectangular strips on each arm of the proposed MS unit cell illustrated in Fig. 3(a). The etched slot gap between the central patch and the rectangular strips of the unit cell generates a capacitive effect, and the series combination of these capacitances reduces the total equivalent capacitance of the MS structure, thereby improving the zero-phase reflection BW. Initially, the source antenna has been optimized and designed based on the operating frequency. An appropriate superstrate structure has been selected according to the BW requirements, and the cavity height of the FP resonator antenna has been chosen according to the resonance condition. In this MS antenna design, a 7×7 array of periodic unit cells has been placed above the modified patch antenna in a superstrate configuration. Here, the superstrate and the ground layers have been separated by a height of sh_1 as illustrated in Fig. 1(a). The resonant conditions of this superstrate-based MS antenna can be expressed in (2) and (3) [2], [3], where, sh_1 is the spacing between the superstrate layer and the ground, φ_s and φ_g are the reflection phases of the superstrate layer and the metal ground plane, respectively, and λ is the operating wavelength in the substrate

$$\varphi_s + \varphi_g - \frac{4\pi sh_1}{\lambda} = 2N\pi,\ N = 0, \pm 1, \pm 2 \ldots \tag{2}$$

$$f = \frac{c}{4\pi sh_1}\left(\varphi_S + \varphi_g - 2N\pi\right). \tag{3}$$

The analysis of a simple patch antenna has been done with a quarter-wave transformer feed for impedance matching in order to minimize the energy reflected from a patch antenna. Later, the

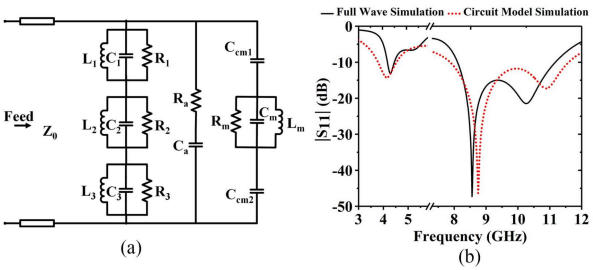

Fig. 4. (a) Equivalent electrical circuit model of the proposed patch antenna with the metasurface as a superstrate. (b) Plot of S_{11} (dB) with respect to frequency using Ansys HFSS simulation versus ADS simulation characteristics comparison.

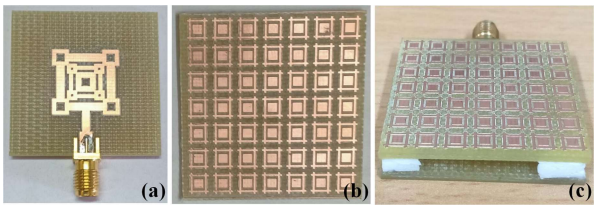

Fig. 5. Proposed fabricated prototype (a) conventional patch, (b) top view of 7×7 order metasurface, and (c) 3-D view of the proposed antenna.

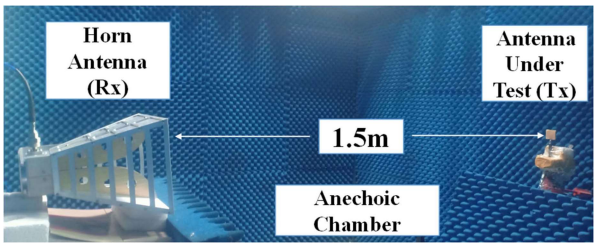

Fig. 6. Radiation pattern measurement of the proposed antenna using an anechoic chamber.

patch was reshaped into square annular-shaped slots placed at the corners for further improvement in the impedance BW as shown in Fig. 3. The slots on the patch improve the input impedance and hence the reflection characteristics ($|S_{11}|$). The selection of various geometries on the patch is attributed to different practical applications. The antenna with quarter-wave transformer feed operates at two distinct frequency regions ranging from 8.3 to 8.51 GHz and 10.19 to 10.87 GHz with a minimum reflection coefficient achieved at 8.42 and 10.4 GHz, respectively. This antenna has been considered as the conventional patch due to its improved impedance matching.

Furthermore, the equivalent electrical circuit model of the MSA, shown in Fig. 4(a), has been subsequently developed using Keysight ADS [13], where the radiating element is represented by a combination of several parallel *RLC* circuits in series [16]. An accurate equivalent circuit analysis is proposed for the design of the MS after taking into account the interlayer mutual coupling effects and the imprecision in predicting the circuit element values. In the circuit models, the dielectric substrate can be modeled as a transmission line with a thickness S_h , and the characteristic impedance can be calculated by $Z_i = {Z_0}/{(\in_r)^{0.5}}$, where $Z_0 = 377\ \Omega$ is the free-space impedance and ε_r is the dielectric constant of the substrate. The circuit representation for the innermost annular patch, the middle slotted region, and the outermost section can be realized by using a parallel combination of R_i, L_i, and C_i ($i = 1, 2,$ and 3), respectively. The effects of the electric field between adjacent elements and the surface current distribution through the MS are considered for establishing the equivalent circuit, including losses for the metasurface. The MS is modeled as an *LC*-resonant circuit employing L_m and C_m for the unit cell. R_m in the Foster canonical form representation for the MS takes care of both radiation and ohmic losses as mentioned earlier [13]. The coupling capacitors are calculated using the parallel-plate capacitor formula $C = \frac{\in_r \in_0 A}{S_h}$ where A is the area of the unit cell of one metasurface layer. Here, C_{cm1} and C_{cm2} are the equivalent coupling capacitances between the neighboring unit cells, along with the vertical and horizontal directions of the MS layer. Besides, the multilayer structures with sh_1 separation between adjacent layers permit mutual coupling, and the effects form the capacitance C_a. The two terminals represent the free space, as shown in Fig. 1(a), on both sides of the compact three-layer MS antenna, having a characteristic impedance of Z_0. The lumped circuit parameters in Fig. 4(a) have been calculated from Keysight ADS simulation analysis and these are: $R_1 = 39.6\ \Omega$, $R_2 = 74.46\ \Omega$, $R_3 = 94.5\ \Omega$, $L_1 = 0.48$ nH, $L_2 = 0.35$ nH, $L_3 = 0.18$ nH, $C_1 = 3.38$ pF, $C_2 = 1.11$ pF, $C_3 = 1.31$ pF, $R_a = 377\ \Omega$, $C_a = 220.65$ pF, $R_m = 94.5\ \Omega$, $C_m = 1.186$ pF, $L_m = 0.273$ nH, $C_{cm1} = 0.35$ pF, $C_{cm2} = 0.35$ pF and $Z_0 = 50\ \Omega$. The comparison of the reflection coefficient responses of the numerical simulation and the circuit model simulation is shown in Fig. 4(b), which offers a good resemblance between the two. It can be seen that the antenna loaded with the MS superstrate layer operates at dual frequency regions with fractional bandwidths of 6.1% and 35.15% at 4.26 and 8.62 GHz, respectively. A maximum return loss of 42 dB has been achieved at 8.62 GHz. This antenna design has been considered as the proposed antenna configuration due to the significantly improved characteristics.

III. Results and Analysis

The proposed antenna has been printed on FR4 dielectric using the LPKF PCB prototyping instrument [17]. The top view of the conventional patch with a 50 Ω SMA connector has been shown in Fig. 5(a). The pictorial representation of the fabricated 7×7 MS layer has been shown in Fig. 5(b). The 3-D view of the proposed fabricated prototype has been illustrated in Fig. 5(c), in which two layers have been separated by foam as the electromagnetic properties of the air spacer and foam are nearly identical along with foam offering mechanical support to the structure. The antenna prototype has been measured in the anechoic chamber using the Keysight FieldFox vector network analyzer N9951A [15]. The far-field radiation characteristics of this antenna have been measured in the anechoic chamber and the experimental set-up has been shown in Fig. 6. In the far-field measurement, the broadband horn antenna [16] has been considered as receiving antenna, while the proposed prototype has been used as the transmitting one.

The simulated and measured reflection coefficient characteristics comparison of the proposed prototype and the reflection coefficient response achieved by the ADS circuit model has been illustrated in Fig. 7(a). The far-field antenna gains and radiation efficiencies of the proposed prototype with respect to frequencies have been shown in Fig. 7(b), where the measured gains have been compared with the simulated one. The experimentally

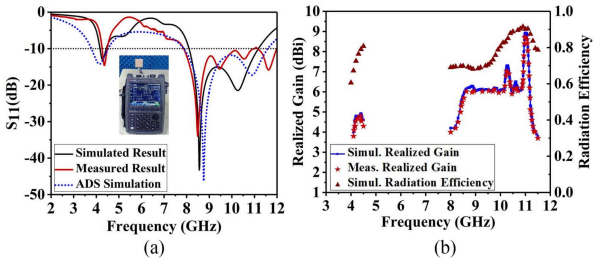

Fig. 7. (a) Plot of the simulated and measured S_{11} (dB) along with circuit model simulation with respect to different frequencies (b) responses of realized gain (dBi) and radiation efficiency with respect to frequencies simultaneously.

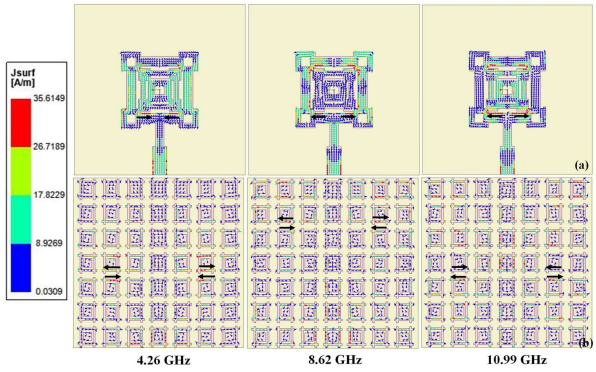

Fig. 8. Surface current distributions at (a) radiating patch (b) 7×7 order MS at different operating frequencies.

measured 10 dB impedance BW has been realized in the frequency ranges of 4.24–4.48 GHz and 7.87–11.01 GHz. Hence, the experimental reflection coefficient response has followed the simulated characteristics as well as the circuit model response.

The surface current distributions of the radiating patch along with the MS layer have been analyzed at 4.26, 8.62, and 10.99 GHz, as illustrated in Fig. 8(a) and (b), respectively. The surface currents are more intense at the slot in the patch and at the aperture of metasurface unit cells, as revealed in Fig. 8. It is further observed that the concentration of surface current at 10.99 GHz is more as compared to other operating frequencies due to maximum field distribution among unit cell slots on the top surface. In the proposed prototype, the maximum simulated realized gain is 8.91 dBi, while the experimentally measured realized gain is 8.72 dBi. Besides, it has been further observed that the maximum radiation efficiency of the proposed antenna is 91% at 10.99 GHz.

The simulated and measured radiation patterns of the proposed antenna along the E-plane ($\varphi = 0°$) and H-plane ($\varphi = 90°$) at 4.26, 8.62, and 10.99 GHz have been illustrated in Fig. 9(a) and (b), respectively. The MS antenna radiates along the boresight direction both in E- and H-planes at all the operating frequencies. It is also evident from Fig. 9 that the measured cross-polarized levels of the proposed antenna remain below 15 dB than those of the copolarized ones in the H-plane at all the operating frequencies. There is a little discrepancy between the simulated and measured results, which may be due to the fabrication tolerances like the copper loss of the FR4 dielectric at the time of polishing, dielectric loss, adaptor, and cable losses incurred during the far-field measurement.

The performance comparison of the proposed MS antenna with some other recently reported high-performance multilayered FP antennas has been shown in Table I. It is seen from

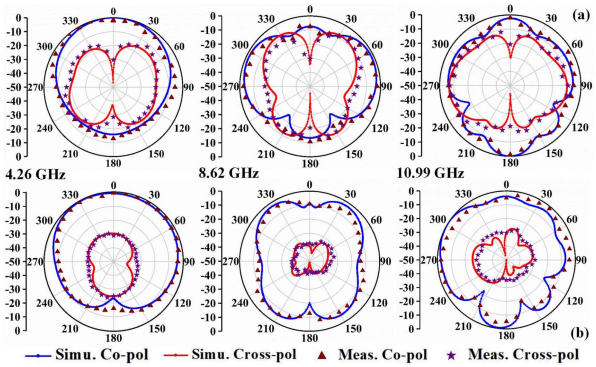

Fig. 9. Radiation pattern (a) E-plane and (b) H-plane copolarized and cross polarized at different operating frequencies within the proposed structure.

TABLE I
COMPARATIVE STUDY OF PROPOSED METASURFACE ANTENNA WITH SOME MULTILAYERED FP ANTENNAS

Ref.	Overall Dimensions	Operating BW (%)	Design Complexity	Gain (dBi)	Efficiency (%)
[5]	$2.2\lambda_0\times2.2\lambda_0\times0.52\lambda_0$	9.42–11.35 (18.58%)	Moderate	11.6	18.8
[6]	$1.87\lambda_0\times1.87\lambda_0\times0.31\lambda_0$	8.25–9.5 (14.7%)	Moderate	11.2	_
[7]	$2.6\lambda_0\times2.6\lambda_0\times0.36\lambda_0$	9.86–10.14 (2.8%)	High	13.4	24.5
[8]	$0.9\lambda_0\times0.9\lambda_0\times0.29\lambda_0$	10.14–10.94 (7.66%)	Low	7.57	_
[20]	$2.6\lambda_0\times2\lambda_0\times0.9\lambda_0$	9.3–11 (16.7%)	Very high	16.6	51
[21]	$2.04\lambda_0\times2.04\lambda_0\times0.55\lambda_0$	7.96–8.14 (2.5%)	Very high	13.25	_
[22]	$2.9\lambda_0\times2.9\lambda_0\times0.5\lambda_0$	9.08–9.86 (8.4%)	High	13.2	_
Prop.	$1.03\lambda_0\times1.03\lambda_0\times0.15\lambda_0$	8.11–11.14 (35.15%)	Low	8.72	91

Table I that the proposed low-profile antenna exhibits a significantly enhanced gain of 8.72 dBi along with improved BW and more compactness. The reported antenna in [8] is low-profile in nature; however, it operates over a narrower BW having lower gain. Some of the reported antennas in [5], [6], [7], [20], [21], and [22] have achieved superior gain, but those were designed in larger dimensions on a substrate with higher relative permittivity.

IV. CONCLUSION

This letter presents a novel dual-band metasurface antenna for applications in C- and X-bands. The antenna operates at two different frequency regions, providing fractional bandwidths of 6.1% and 35.15% at 4.26 and 8.62 GHz, respectively. A maximum realized gain of 8.91 dBi and a maximum radiation efficiency of 91% have been achieved at 10.99 GHz. The equivalent circuit model with the component values of the modified slotted patch antenna and the same patch with MS as a superstrate has been subsequently developed in the manuscript. The experimentally measured impedance response of the fabricated prototype offers a good match with the simulated and circuit model responses of the antenna, thereby validating the design. The measured far-field characteristics of the antenna are also in good resemblance to the simulated ones. The antenna can be utilized for both C-band and X-band applications like military purposes, satellite communication, medical applications, etc.

REFERENCES

[1] H. Li, G. Wang, X. Gao, J. Liang, and H. Hou, "A novel metasurface for dual-mode and dual-band flat high-gain antenna application," *IEEE Trans. Antennas Propag.*, vol. 66, no. 7, pp. 3706–3711, Jul. 2018.

[2] J. Zhang, S. Yan, and G. A. E. Vandenbosch, "Radial CRLH-TL-based dual-band antenna with frequency agility," *IEEE Trans. Antennas Propag.*, vol. 68, no. 7, pp. 5664–5669, Jul. 2020.

[3] H. Yang and X. Liu, "Wearable dual-band and dual-polarized textile antenna for on- and off-body communications," *IEEE Antennas Wireless Propag. Lett.*, vol. 19, no. 12, pp. 2324–2328, Dec. 2020.

[4] J. Canet-Ferrer, *Metamaterials and Metasurfaces*. London, U.K.: IntechOpen, 2019, ch. 4, pp. 63–85, doi: 10.5772/intechopen.73359.

[5] Y. Zheng et al., "Wideband gain enhancement and RCS reduction of fabry–perot resonator antenna with chessboard arranged metamaterial superstrate," *IEEE Trans. Antennas Propag.*, vol. 66, no. 2, pp. 590–599, Feb. 2018.

[6] K. Li, Y. Liu, Y. Jia, and Y. J. Guo, "A circularly polarized high-gain antenna with low RCS over a wideband using chessboard polarization conversion metasurfaces," *IEEE Trans. Antennas Propag.*, vol. 65, no. 8, pp. 4288–4292, Aug. 2017.

[7] Y. Wang and A. Zhang, "Dual circularly polarized Fabry–Perot resonator antenna employing a polarization conversion metasurface," *IEEE Access*, vol. 9, pp. 44881–44887, 2021.

[8] D. Samantaray and S. Bhattacharyya, "A gain-enhanced slotted patch antenna using metasurface as superstrate configuration," *IEEE Trans. Antennas Propag.*, vol. 68, no. 9, pp. 6548–6556, Sep. 2020.

[9] Y. Zheng et al., "Wideband gain enhancement and RCS reduction of Fabry–Perot resonator antenna with chessboard arranged metamaterial superstrate," *IEEE Trans. Antennas Propag.*, vol. 66, no. 2, pp. 590–599, Feb. 2018.

[10] K. Konstantinidis, A. P. Feresidis, and P. S. Hall, "Broadband subwavelength profile high-gain antennas based on multi-layer metasurfaces," *IEEE Trans. Antennas Propag.,* vol. 63, no. 1, pp. 423–427, Jan. 2015.

[11] A. Iqbal, M. A. Selmi, L. F. Abdulrazak, O. A. Saraereh, N. K. Mallat, and A. Smida, "A compact substrate integrated waveguide cavity-backed self-triplexing antenna," *IEEE Trans. Circuits Syst. II: Exp. Briefs*, vol. 67, no. 11, pp. 2362–2366, Nov. 2020.

[12] Ansys Electronics Desktop, R1, 2019, ANSYS Corporation.

[13] Keysight. Advanced Design System (ADS). Accessed: 2021. [Online]. Available: https://www.keysight.com/in/en/products/software/pathwave-design-software/pathwave-advanced-design-system.html

[14] A. B. Numan and M. S. Sharawi, "Extraction of material parameters for metamaterials using a full-wave simulator [Education Column]," *IEEE Antennas Propag. Mag.*, vol. 55, no. 5, pp. 202–211, Oct. 2013.

[15] Y. -F. Cheng, J. Feng, C. Liao, and X. Ding, "Analysis and design of wideband low-RCS wide-scan phased array with AMC ground," *IEEE Antennas Wireless Propag. Lett.*, vol. 20, no. 2, pp. 209–213, Feb. 2021.

[16] S. B. T. Wang, A. M. Niknejad, and R. W. Brodersen, "Circuit modeling methodology for UWB omnidirectional small antennas," *IEEE J. Sel. Areas Commun.*, vol. 24, no. 4, pp. 871–877, Apr. 2006.

[17] LPKF PCB Prototyping Instrument model S103.

[18] Keysight Technologies, N9951A Vector Network Analyzers Data Sheet, 2019. [Online]. Available: http://www.keysight.com

[19] Applied.cg, Broadband Horn Antenna, 1GHz-18GHz, Haryana, India.

[20] X. Liu, Z. Yan, E. Wang, T. Zhang, and F. Fan, "Magnetoelectric dipole-fed Fabry–Perot antenna with wideband RCS reduction based on multilayer metasurface," *IEEE Antennas Wireless Propag. Lett.*, vol. 20, no. 7, pp. 1342–1346, Jul. 2021.

[21] C. Chen, Z. Liu, H. Wang, and Y. Guo, "Metamaterial-inspired self-polarizing dual-band dual-orthogonal circularly polarized Fabry–Pérot resonator antennas," *IEEE Trans. Antennas Propag.*, vol. 67, no. 2, pp. 1329–1334, Feb. 2019.

[22] Y.-J. Zheng, J. Gao, X.-Y. Cao, S.-J. Li, and W.-Q. Li, "Wideband RCS reduction and gain enhancement microstrip antenna using chessboard configuration superstrate," *Microw. Opt. Technol. Lett.*, vol. 57, no. 7, pp. 1738–1741, Jul. 2015.